ELSEVIER

Astroparticle Physics 6 (1997) 143-153

Astroparticle
Physics

The shapes of the atmospheric Cherenkov light images from extensive air showers

EAS-TOP Collaboration

M. Aglietta [b,c], B. Alessandro [c], P. Antonioli [g], F. Arneodo [c,f], L. Bergamasco [a,c], M. Bertaina [a,c], C. Castagnoli [a,c], A. Castellina [b,c], A. Chiavassa [a,c], G. Cini Castagnoli [a,c], B. D'Ettorre Piazzoli [d], G. Di Sciascio [d], W. Fulgione [b,c], P. Galeotti [a,c], P.L. Ghia [b,c], M. Iacovacci [d], G. Mannocchi [b,c], C. Melagrana [a,c], N. Mengotti Silva [c,e], C. Morello [b,c,*], G. Navarra [a,c], L. Riccati [c], O. Saavedra [a,c], G.C. Trinchero [b,c], P. Vallania [b,c], S. Vernetto [b,c]

[a] *Dipartimento di Fisica Generale dell' Universita', Torino, Italy*
[b] *Istituto di Cosmo-Geofisica del CNR, Torino, Italy*
[c] *Istituto Nazionale di Fisica Nucleare, Torino, Italy*
[d] *Dipartimento di Scienze Fisiche dell' Universita' di Napoli and INFN, Napoli, Italy*
[e] *Instituto de Fisica, Universidad Estadual de Campinas, SP, Brazil*
[f] *Dipartimento di Fisica dell' Universita', L'Aquila, Italy*
[g] *Istituto Nazionale di Fisica Nucleare, Bologna, Italy*

Received 21 March 1996; revised 6 June 1996; accepted 9 July 1996

Abstract

Experimental results on the shapes of atmospheric Cherenkov light images from Extensive Air Showers at $E_0 = 10^{13}-10^{14}$ eV are presented. The results are based on data obtained by the first element of the Cherenkov light array of the EAS-TOP experiment at Campo Imperatore (2005 m a.s.l., National Gran Sasso Laboratories, Italy). Images are obtained with pixel field of view $\omega = 1.5 \times 10^{-5}$ sr and full field of view $\Omega \approx 10^{-3}$ sr. The shapes of the images agree with the expectations and their fluctuations are large and significant. Experimental data on the dependence of the image shapes on the detection geometry are reported. The images are well reproduced by two independent side by side detectors, within measured accuracies. Such accuracies ($\approx$ 15% for large photoelectron content) define the level at which each pixel content is related to the shower structure. The presence of events characterized by patterns with multiple structures is proved. It is shown that such features are related to physical fluctuations of the shower structure.

---

1. Introduction

Cosmic rays and their interactions at primary energies $E_0 > 10^{14}$ eV are studied through the detection of the cascades they induce in the atmosphere (Extensive Air Showers, EAS) by means of ground based observatories (i.e. by observations at fixed target thickness). Different EAS components can be recorded, but the main limitation to such experiments arises from the lack of information on the shower

---

[*] Corresponding author.

PII S0927-6505(96)00050-3

development above the observation level. This is related to the rate of energy release by the primary particle and represents therefore an important datum for the identification of the primary itself, the measurement of its energy and of its interaction properties.

The main tool for obtaining such information is provided by the detection of the Cherenkov light (C.l.) signal produced in the atmosphere by the ultrarelativistic electrons and positrons of the cascade. In fact, while the total C.l. flux provides a measurement of the total energy released above the observation level, the structure of the C.l. signal (lateral, temporal and angular distributions) is related to the development of the cascade. In particular the angular distribution, i.e. the shape of the Cherenkov image, contains the information on the direction of production of the light, and therefore on the detection geometry and on the electron density in space, i.e. the EAS longitudinal development and lateral distribution.

The recognition of the physical information achievable through the study of the angular distribution of the light across the C.l. image occurred in the sixties, when first calculations [1] and simulations [2] were performed. A first pioneering experiment was carried out by means of an image intensifier system [3]. The experimental difficulties limited, however, for many years the exploitation of the technique, and the information on the EAS longitudinal profile (atmospheric depth of maximum development, $X_{\max}$) was mainly obtained through the analysis of the temporal shape of the pulses [4,5] and, at the extremely high energies, through the atmospheric fluorescent light technique [6].

More recently the rejection of a large fraction of isotropic hadron primaries versus γ-ray primaries with arrival direction from a point source has been achieved through the analysis of the C.l. images. The technique has lead to the detection of TeV gamma ray signals from the Crab Nebula [7] and Markarian 421 [8]. A new window has thus been opened to the research in high energy astrophysics.

From the experimental point of view new techniques are now available, such as arrays of photomultipliers [9–12], multi-channel photomultipliers [13,14] and further possibilities are foreseen for the future [15,16]. Moreover arrays of C.l. detectors can operate in coincidence with detectors of other EAS components (electrons, GeV and TeV muons, hadrons), thus providing a complete information on the recorded events [17–19].

The integration of angular measurements of atmospheric Cherenkov light with the information of a complete EAS array is within the aims of the EAS-TOP experiment at Campo Imperatore (2005 m a.s.l., above the underground Gran Sasso laboratories [20,21]).

To meet the required resolution in the spatial reconstruction of the events, C.l. measurements are performed in stereoscopic mode, by means of an array of eight steerable telescopes (four in operation, and four on advanced stage of construction) separated of about 60 m from each other. Each telescope loads:

- two large angle detectors ($\cong 0.16$ sr full field of view) to provide a good measurement of the total C.l. signal and a large effective detection area;
- an high resolution ($\omega = 1.5 \times 10^{-5}$ sr) imaging detector based on multi-channel photomultipliers to investigate the angular distribution of the light across the Cherenkov spot.

In the present paper the data obtained from the imaging detectors are used to discuss the shapes of the C.l. images, the accuracy and significance of the information they contain and the influences of geometrical and local effects. It is shown that besides the average parameters used in V.H.E. γ-ray astronomy [22], the whole pattern of the light spots carries significant informations on the shower structure. Complex images are also observed and they reflect real EAS structures.

The data have been recorded by two imaging detectors located side by side on the same mounting (the first element of the array), and with parallel optic axis. The EAS primary energies are between 10^{13} and 10^{14} eV.

First results on the telescope operation, on the detector resolutions, and on the shapes of the C.l. images have been reported in Refs. [23–28].

2. The detectors

The two imaging detectors consist of multi-channel photomultipliers Philips XP1704 (hereafter referred as A) and XP4702 (referred as B) having respectively useful photocathode areas of 6 cm^2 (96 pixels on an almost circular pattern) and 4 cm^2 (64 pixels on a square matrix) [29]. Pixel dimensions are 0.25×0.25 cm^2. The photomultipliers are positioned at the foci of parabolic light receivers 90 cm diameter, 64.5 cm focal length, for total apertures of 1.4×10^{-3} sr (A) and 9.6×10^{-4} sr (B), the field of view of each pixel being 1.5×10^{-5} sr. The distance between the optic axis of the two detectors is 1 m.

Due to the large apertures of optical systems, the effects of aberrations (maily coma) have been calculated and measured: for a point source at infinity, 0.8° off the optic axis, 90% of the light falls inside one pixel's area.

The pointing and the orientation of the photocathodes are measured and monitored through the observation of stars crossing the fields of view of the detectors. On the analyzed data set the pointing of each individual pixel is known with accuracy better than 0.1°.

The pixel outputs are read through ADCs CAEN C205 with sensitivity 0.033 pC/count (15 bit dynamic range) and integral non linearity < 0.2 pC.

The conversion factor between ADC counts and number of photoelectrons (2 ADC counts/photoelectron) has been obtained from the nominal gain of the photomultipliers at the operating H.V. (8×10^5 and 2×10^6) and from the attenuation of the 45 m cables connecting the pixel outputs to the ADCs.

The gate width is 70 ns, being 0.5 photoelectron/pixel the average accumulated background from the nightsky inside the integration time.

The trigger condition is provided by the coincidence (resolving time 30 ns) between the anode signals of detector A and of a photomultiplier XP3462B, positioned at the focus of a similar light collector, housed on the same mounting and having the field of view reduced to 10^{-3} sr. The triggering threshold is set at 50 photoelectrons on each detector. The trigger rate is 0.4 Hz with the telescope axis pointing to the zenith.

The mean recorded number of photoelectrons/event is $\langle N_{\rm phe} \rangle \approx 200$; the fraction of coincidences with the EAS electromagnetic (e.m.) detector of EAS-TOP, operating in fourfold coincidence mode, is $\approx 8\%$.[1] The typical primary energy of the C.l. events (from trigger rate, number of collected photoelectrons, and coincidence rate with the EAS e.m. detector) is $E_0 = (2\text{–}3) \times 10^{13}$ eV.

The image preparation consists of a three steps procedure: subtraction of the ADC pedestals, equalization of the channel gains and zeroing of the pedestal fluctuations.

The ADC pedestals are measured under normal operating conditions before and after each run by feeding the ADCs with artificial triggers to integrate the nightsky background. The pedestals are also determined directly from the data: each image involves, in general, only 10–15 pixels and the differential charge distribution for a particular channel shows a clear maximum centered on the pedestal value. The two values agree within 1–2 ADC counts, the widths of both distributions being 2–3 counts. The latter method has been preferred in the following analysis as it compensates for possible drifts during data taking.

The relative gains of the individual channels are equalized by normalizing their mean number of photoelectrons recorded in the whole observation to the overall mean value. The result of this calibration agrees within 20% with the relative gains obtained from the measurements of the pixel nightsky currents and within 25% with the pixel gains provided by the photomultiplier manufacturer. The procedure is applied to both detectors and, on average, it implies a 10% gain normalization between the two photomultipliers.

The channels whose pulse charge is less than three ADC counts (equal to the observed r.m.s. value of the pedestals) are set to zero for all the analysis unless for the one described in Section 3.3 where no zeroing is applied.

Only events with the maximum number of photoelectrons recorded by an internal pixel of photocathode B have been considered for further analysis.

---

[1] The detection efficiency of the detector of the e.m. component operating in four-fold coincidence mode increases from 20% at primary energy $E_0 \approx 25$ TeV to 80% at $E_0 \approx 55$ TeV, and in seven-fold coincidence mode from 20% at $E_0 \approx 55$ TeV to 80% at $E_0 \approx 110$ TeV (for primary protons in the vertical direction). The detection geometry is reconstructed with a resolution of $\Delta r \approx 10$ m in the core location and $\Delta\beta \approx 0.5°$ in the arrival direction at $Ne = 10^5$ particles, i.e. $E_0 \approx 300$ TeV.

3. The experimental results

The study of the shapes of the images, of their fluctuations and of their physical content is achieved through the parallel analysis of the events registered by the two detectors with the telescope looking to the zenith and the comparison with the expectations from a full M.C. simulation.

In concerns: the general features of the images, the parameters used in the field of V.H.E. γ-ray astronomy and the influence of the detection geometry (Section 3.1), the measurement of the direction of light maximum (Section 3.2), the physical content of the observed light patterns (Section 3.3) and the existence of events with complex features (Section 3.4).

The simulation of the Cherenkov photon emission by the electrons and positrons of the cascade has been obtained by a routine run by means of the GEANT code (version 3.21) [30] reproducing the EAS cascade in the atmosphere. The hadronic part of the cascade has been simulated by the GEANT/FLUKA interface. The atmosphere has been divided into 16 layers with scaling densities, the light absorption in air is taken from Ref. [31]. Primary protons are uniformly generated with spectral index $\gamma = 2.7$ in a cone 10 degrees aperture around the optical axis. The detector response (optics and electronics) is included following the data reported in Section 2 and, concerning the fluctuations, in the Eq. (5) of this paper. The same procedures of analysis are applied to the simulated and experimental events.

3.1. General features and parameters of the image

A first information on the concentration of the images is shown in Fig. 1a, where the fraction of the total light signal contained inside a given opening angle around the pixel with the maximum photoelectron content is drawn. On average, 90% of the signal is contained inside 1.3°, as expected from calculations [1,2]. A few individual events are also drawn, to show that fluctuations among different events are rather large. For events obtained with the described simulation, the same plot is presented in Fig. 1b: the mean value and the fluctuations of the experimental data are well reproduced.

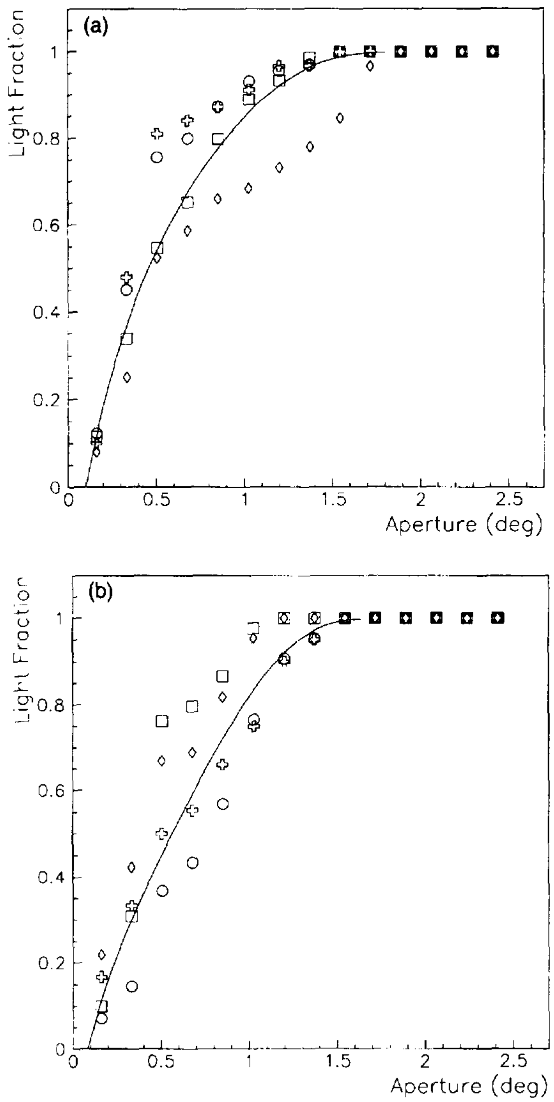

Fig. 1. Fraction of the total light signal inside a given opening angle around the brightest channel: the plot shows the trend of the mean value (solid line) and of four individual events. (a) real events, (b) simulated ones.

The general features of the images have been studied following the parameters introduced in Ref. [22]: length (L), width (W), azwidth (Az), i.e. the dispersions of the distributions of the recorded number of photoelectrons with respect to the major (L) and minor (W) axis of the image, and to the azimuthal angle with respect to the axis of the detector (Az). The experimental mean values and the s.d. of the parameters are reported on Table 1.

Table 1
Experimental mean values and s.d. of the parameters length, width and azwidth. The s.d. of the parameters for $N_{\mathrm{phe}} = 400$ are derived from Eqs. (1)–(3)

Parameter	Mean value (deg.)	s.d.	s.d. ($N_{\mathrm{phe}} = 400$)
Length	0.501	0.103	0.056
Width	0.326	0.081	0.050
Azwidth	0.432	0.106	0.068

The comparison of the measurement of the same parameter on the two photomultipliers provides the accuracy of its determination. As an example, the scatter plot of the lengths, as measured by the two detectors (A, B), is shown in Fig. 2 for events with total number of photoelectrons (N_{phe}) on both photocathodes > 150. The dependence of the standard deviation of the distribution of the differences be-

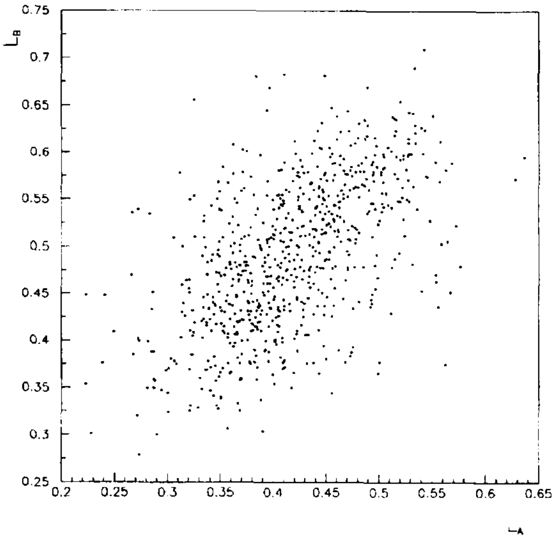

Fig. 2. Scatter plot of the parameter length as measured by the two detectors for events with $N_{\mathrm{phe}} > 150$. The correlation coefficient is $r = 0.57 \pm 0.03$.

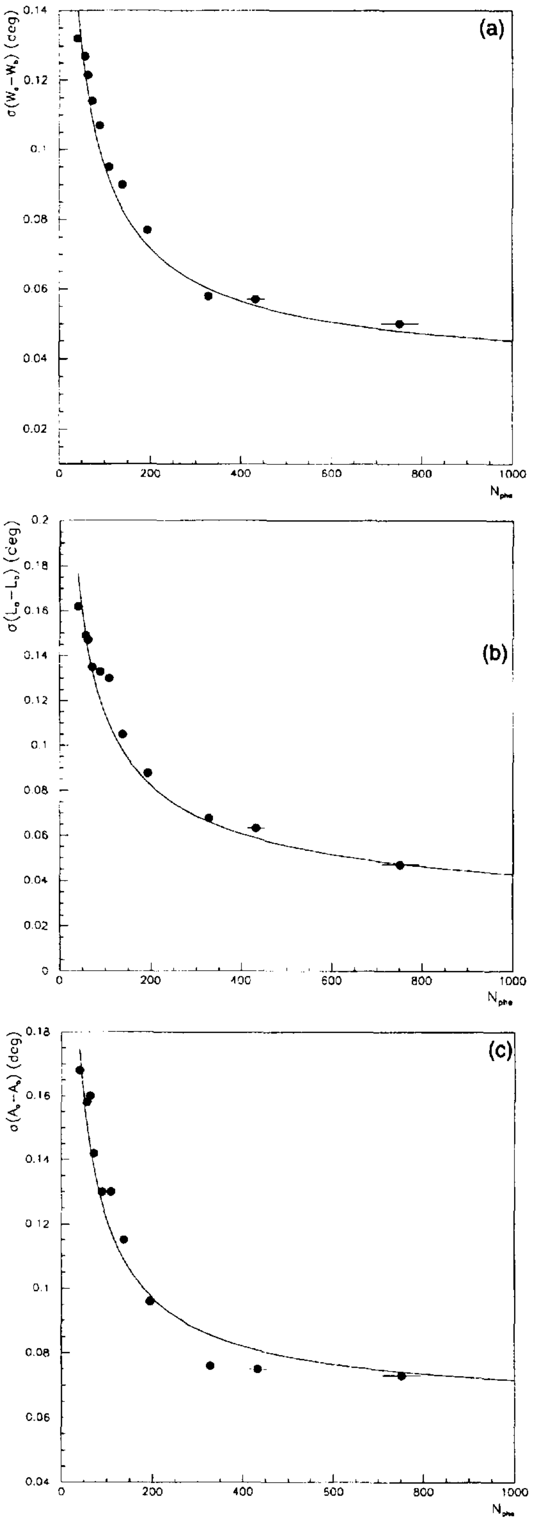

Fig. 3. Dependence of the standard deviation of the distribution of the differences between the parameters measured on the two detectors versus the average number of photoelectrons on the photocathodes: width (a), length (b) and azwidth (c).

tween the two measurements on the average number of collected photoelectrons is shown in Fig. 3(a, b, c) for the parameters length, width and azwidth. The fits lead to the expressions:

$$\sigma_L^2 = (1.1)^2/N_{\text{phe}} + (0.01)^2\ \text{deg}^2, \qquad (1)$$

$$\sigma_W^2 = (0.9)^2 N_{\text{phe}} + (0.02)^2\ \text{deg}^2, \qquad (2)$$

$$\sigma_{\text{Az}}^2 = (1.1)^2 N_{\text{phe}} + (0.04)^2\ \text{deg}^2, \qquad (3)$$

for the variances of the parameters measured on a single imaging device for fixed N_{phe}. The standard deviations of the parameters for $N_{\text{phe}} = 400$ are also reported in Table 1, showing that about 50% of the contribution to the dispersions of the experimental values of the parameters is of physical origin.

The influence of the detection geometry on the parameters (L, W, Az) has been studied by analyzing their dependencies on the tilt angle (α) between the shower axis (obtained by means of the e.m. particle detector) and the optical axis of the C.I. detector. Such dependencies are shown in Fig. 4(a, b, c), proving that EAS propagating along the optical axis of the detector have smaller parameters. Also shown in Fig. 4 are the behaviors expected from the described simulation. The trends of the measured and simulated data agree; small differences in the absolute values are due to the uncertainties in the angular measurements of the e.m. detector.

3.2. Direction of light maximum

The atmospheric depth of the shower maximum (X_{max}) can be derived from the measurement of the arrival direction of the maximum light intensity (C_{max}). The precision on the measurement of X_{max} is therefore related to the experimental accuracy when measuring C_{max} on single events.

On our analysis the direction C_{max} is defined as the position on the photocathode of the barycenter of the four brightest pixels.

The error in the measurement of C_{max} is obtained from the distribution of the angular distances be-

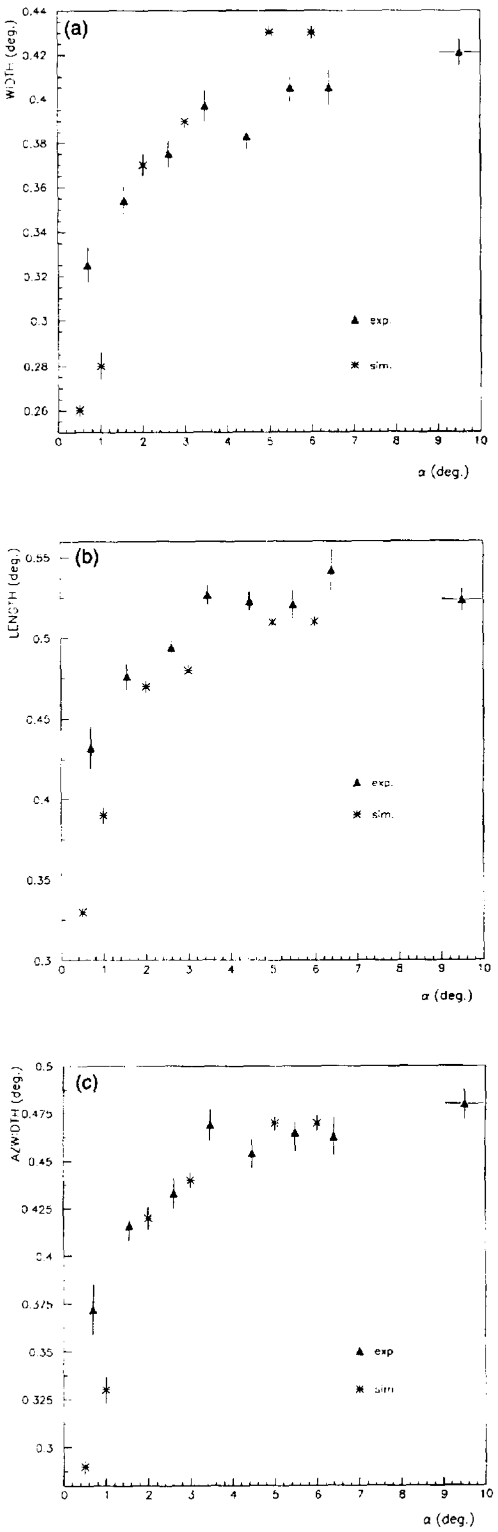

Fig. 4. Measured and simulated dependence of the parameters width (a), length (b) and azwidth (c) on the tilt angle (α) between the shower axis and the optical axis of the detector.

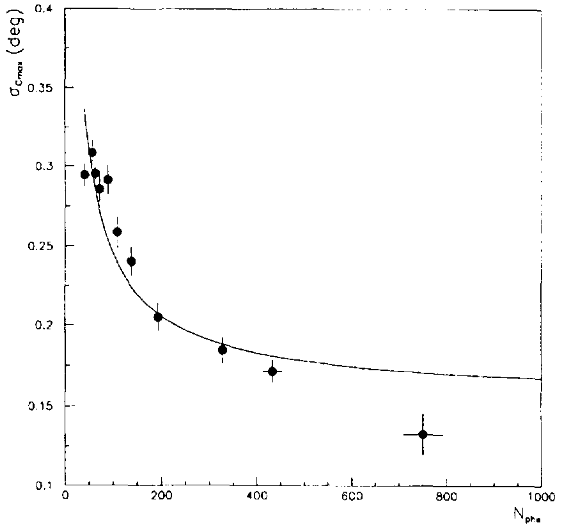

Fig. 5. Standard deviation of the bidimensional gaussian error distribution in the measurement of the arrival direction of the light maximum ($C_{\max}$) on a single detector versus N_{phe}.

tween the two measurements. Fig. 5 shows the dependence of $\sigma_{C_{\max}}$ (standard deviation of the bidimensional gaussian error distribution on a single imaging device) on the mean number of photoelectrons detected on the photocathodes. The trend can be expressed by the relation:

$$\sigma_{C_{\max}}^2 = (2.0)^2/N_{\text{phe}} + (0.1)^2 \text{ deg}^2. \qquad (4)$$

For large values of N_{phe} the asymptotic value of $\sigma_{C_{\max}}$ ($\approx 0.1°$) is about half of the pixel dimensions. The corresponding error in reconstructing the direction of light maximum for individual events from two observation points is $\approx 0.2°$.

3.3. Light pattern on the photocathodes

The study of the physical information carried by the full pattern of the image requires the separation of the contribution to the shape due to the EAS structure from the fluctuations introduced by the local and instrumental effects and it has been performed through the comparison between the light patterns detected on the two photocathodes. The pixel grid of photomultiplier B has been projected on the pixel grid of photomultiplier A. The photoelectrons of each pixel of detector B have been re-distributed over the 'new' ones assuming a uniform distribution inside the pixels. The procedure leads to two photocathodes of 60 pixels fully superimposed and the comparison between the number of photoelectrons recorded on the corresponding channels (n_{pheA}, n_{pheB}) can thus be obtained. Fig. 6 shows the dependence of the standard deviation of the distribution of $(n_{\text{pheA}} - n_{\text{pheB}})/(n_{\text{pheA}})$ on the mean number

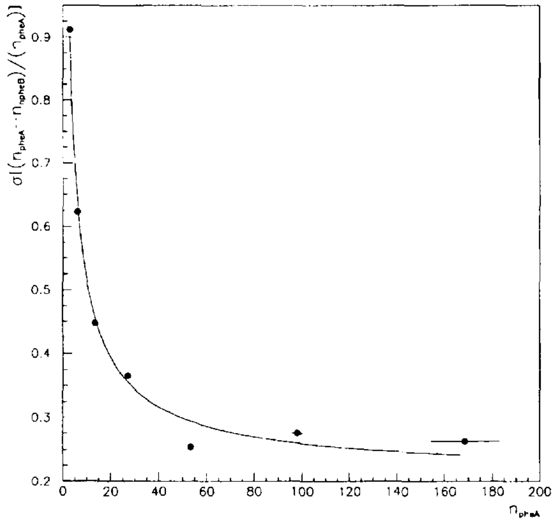

Fig. 6. Dependence of the s.d. of $(n_{\text{pheA}} - n_{\text{pheB}})/(n_{\text{pheA}})$ on the number of photoelectrons recorded on the channels of detector A.

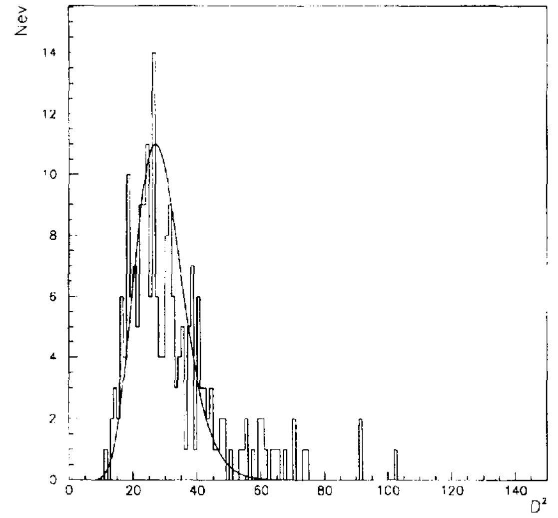

Fig. 7. D^2 distribution (see Eq. (6)) for events with $N_{\text{phe}} \geqslant 100$ obtained by using the 30 brightest channels selected on detector A; the distribution is compared with the χ^2 distribution with 29 degrees of freedom (full line).

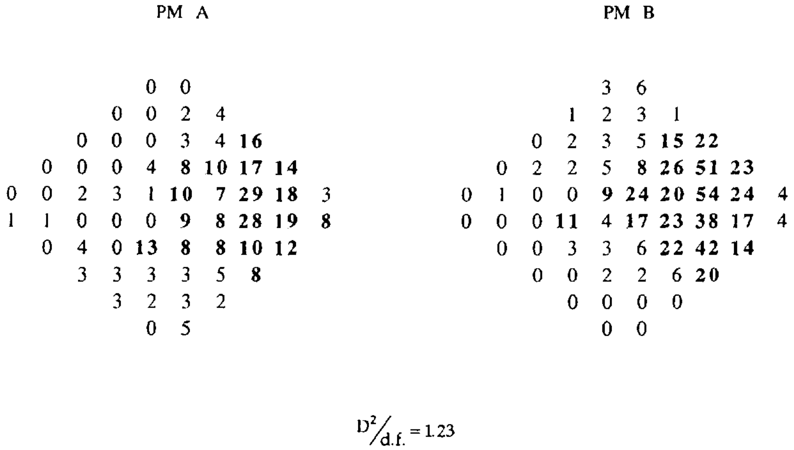

Fig. 8. Cherenkov light images, expressed in number of photoelectrons on each channel, of the same shower as observed by the two detectors (A, B). The photoelectron content of the channels belonging to different clusters, as identified by the procedure discussed in the text, are shown in bold. The D^2 value is calculated on 60 channels.

of photoelectrons on the channels of photomultiplier A. The fit leads to the expression:

$$\sigma^2/n_{\text{phe}}^2 = (1.5)^2/n_{\text{phe}} + (0.15)^2 \tag{5}$$

for the dispersion in the photoelectron counting of each individual channel assuming $\sigma_{\text{npheA}} = \sigma_{\text{npheB}}$; n_{phe} is the number of photoelectrons on the individual channels. The asymptotic value of 15% is mostly related to the uncertainties in the described procedure of relative gain adjustment.

Eq. (5) represents therefore, in our measurement, the accuracy in reproducing C.l. images with pixel resolution $\omega = 1.5 \times 10^{-5}$ sr, including instrumental effects, light collection and photoelectron fluctuations, and 'local' effects due to light produced in the lower 100 m of atmosphere, where the fields of view of the two detectors are not fully overlapped.

A point by point comparison between the images of the same event obtained by the two detectors can be achieved by means of the distribution of the differences between the photoelectron counting of corresponding channels, weighted by the s.d. derived from Eq. (5):

$$D^2 = \sum_i \left\{ \frac{1}{2\sigma_i^2} \left[n_{\text{pheA}}^i - n_{\text{pheB}}^i \right]^2 \right\} \tag{6}$$

where, to avoid the influence on D^2 of the channels not affected by the image, the summation is extended

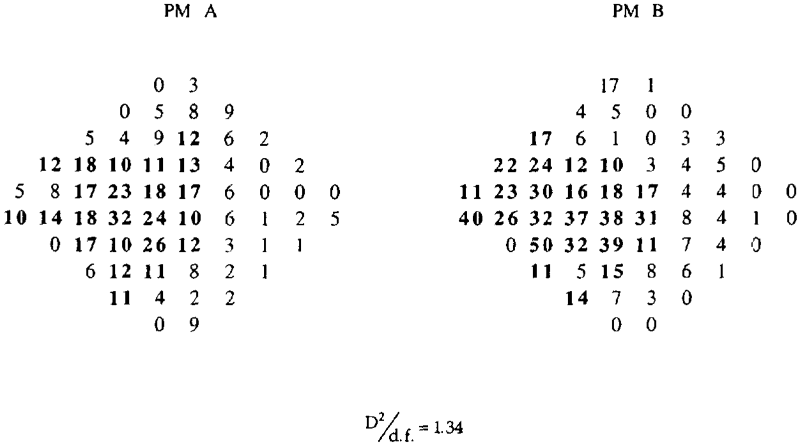

Fig. 9. See caption of Fig. 8.

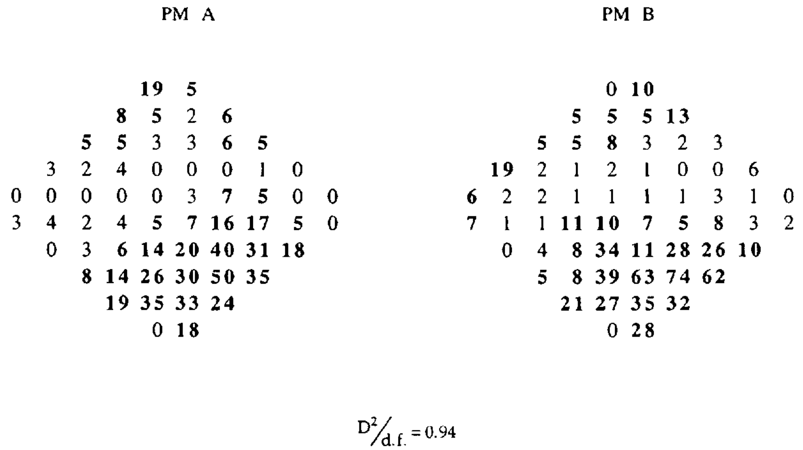

Fig. 10. 'Multistructured' event as observed by the two detectors (A, B). See also the caption of Fig. 8.

over the 30 brightest channels selected on detector A. The D^2 distribution is shown in Fig. 7 for events with $N_{\text{phe}} \geq 100$: it follows the χ^2 distribution (29 d.f.), showing that practically all individual events are well reproduced on the two detectors.

We can conclude that the photon content of each pixel, i.e. the whole pattern of the image, contains a significant information on the shower at the accuracy level described by Eq. (5).

Examples of events as seen by the two photomultipliers (A, B) are displayed in Figs. 8 and 9. The agreement between the shapes of the images, visible by eye, is confirmed by the values of $D^2/\text{d.f.}$

3.4. '*Multistructured*' images

Structures involving a number of photoelectrons (n_{phe}) from the statistical point of view significantly larger than in Eq. (5) reflect therefore physical characteristics of the Cherenkov light spot.

Fig. 11 show images characterized by complex patterns indicating two different concentrations of

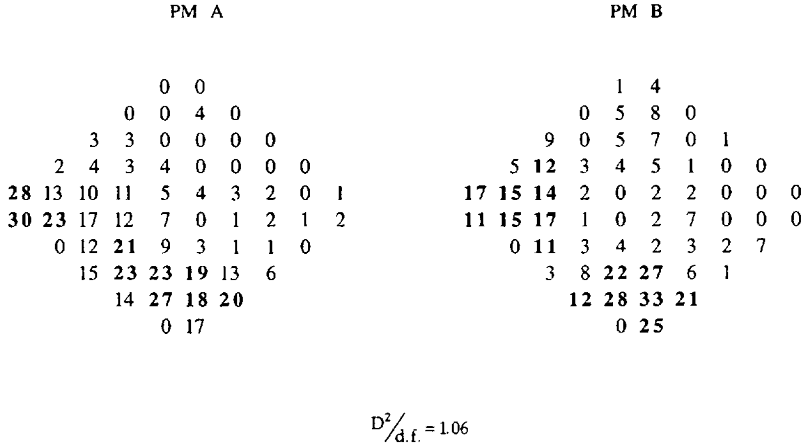

Fig. 11. See caption of Fig. 10.

light on the photocathodes of both detectors. The search for images with multiple light clusters ('multistructured' events) is performed independently on the two photocathodes. A cluster is defined as any combination of two or more adjacent channels whose photoelectron content exceeds by at least 2 s.d. a threshold value defining the separation between the candidate clusters. The fluctuations are obtained from Eq. (5). The search is performed by lowering the quoted threshold from the photoelectron content of the brightest channel to a minimum value set at 2.5 s.d. above the channel pedestals. Each candidate cluster is classified following its higher significance. The 2 s.d. separation level guaranties a good rejection of multiple structures generated by the sole fluctuations of the channel amplitudes.

The two secondary clusters of the events shown in Figs. 10 and 11 are identified with significances respectively of 4.9 s.d. (Fig. 10, PM A), 3.8 s.d. (Fig. 10, PM B) and 3.5 s.d. (Fig. 11, PM A), 4.1 s.d. (Fig. 11, PM B) with respect to the probability of being generated by the channel fluctuations and hence they are expected to be of physical origin.

On other side the D^2 values (Eq. (6)) obtained from the comparison of the images (0.94/d.f. and 1.06/d.f.) demonstrate also these events are well consistent on the two detectors within the uncertainties of Eq. (5).

With the described criterium, on the data set presented in this paper, 10% of the events are classified as 'multistructured' events in coincidence on both detectors. This value is 7 s.d. above the rate of multistructured events expected on both detectors by chance, as it can be obtained from the rate of multistructured images found independently on the two single detectors. This further confirms the non instrumental, non statistical and non local origin of the observed composite structures. As we can see from Figs. 10 and 11 such substructures are characterized by 50–100 photoelectrons that are detected, if occurring the best geometrical conditions, from a 100 GeV e.m. cascade.

The maximum rate of cosmic ray primaries of such energy in our detector is ≈ 40 Hz, and the probability for one of them to occur inside the ADC gate (70 ns) is less than 10^{-5}. The possibility for such a double structure to be due to accidental coincidences is thus excluded.

The angular distance of the two spots can be due to a radial separation (i.e. connected to substructures in the particle lateral distribution) or to a longitudinal separation (i.e. large fluctuation in the interaction length of a secondary). Data from different observation points can discriminate the two cases.

An indication of the presence of multistructured patterns in atmospheric C.l. images was reported in Ref. [32]. Structures in the nanosecond temporal profile of the C.l. signal, possibly of the same origin of the present ones, were reported in Refs. [33–35].

4. Conclusions

Experimental data on the shapes of the atmospheric Cherenkov light images from EAS at $E_0 = 10^{13}$–10^{14} eV, observed with pixel f.o.v. of 1.5×10^{-5} sr, are presented.

The images are well reproduced by two side by side independent detectors, inside measured errors ($\approx 15\%$, besides the photoelectron fluctuations). At such accuracy level the full pattern of the image is representative of the atmospheric shower.

Events with complex light patterns are recorded at our energy threshold at a rate of 10% of the total rate. It is shown that such structures are of physical origin, connected with the longitudinal EAS development or the EAS structure.

The parameters characterizing the shapes of the light spots (length, width and azwidth) are measured with accuracy $\lesssim 20\%$. The resolutions improve when increasing the number of photoelectrons, being on average $< 13\%$ for $N_{\mathrm{phe}} > 150$.

The dependence of the parameters (L, W, Az) on the detection geometry has been measured and follows the expectations: the images of showers with axis parallel to the optical axis of the detector are characterized by parameters with smaller mean values. This effect has been calculated [22], and exploited in the VHE γ-ray astronomy applications [7,8].

The direction of the maximum light intensity ($C_{\max}$) is detected (besides photoelectron fluctuations) with an accuracy of ≈ 0.1 deg. The relative error in reconstructing its direction from two observation points (0.2 deg.) means that with three-four observation points separated of 50–100 m, as for the

EAS-TOP Cherenkov array, a resolution on the atmospheric depth of $C_{\max}$ of $\Delta C_{\max} < 30\ \mathrm{g/cm^2}$ can be obtained in individual events. This resolution has to be compared with the average separation between the EAS maxima originated by different primaries; in the case of protons and iron initiated showers such separation is $\cong 100\ \mathrm{g/cm^2}$.

Acknowledgements

The continuous cooperation of the director and of the staff of the Gran Sasso National Laboratories as well as the technical assistance of C. Barattia, R. Bertoni, M. Canonico, G. Giuliani, A. Giuliano and G. Pirali are gratefully acknowledged.

References

[1] V.I. Zatsepin et al., Sov. Phys. JEPT 20 (1965) 459.
[2] C. Castagnoli et al., Nuovo Cimento B 9 (1972) 213.
[3] D.A. Hill and N.A. Porter, Nature 191 (1961) 690.
[4] C. Castagnoli et al., Phys. Rev. 160 (1967) 1186.
[5] Yu.A. Fomin et al., Proc. XVIII Int. Cosmic Ray Conf. 4, Bangalore (1983) p. 67.
[6] D.J. Bird et al., Phys. Rev. Lett. 71 (1993) 3401.
[7] T.C. Weekes et al., Astrophys. J. 342 (1989) 379.
[8] M. Punch et al., Nature 358 (1992) 477.
[9] M.F. Cawley et al., Nucl. Instr. Meth. A 264 (1988) 64.
[10] B. Degrange et al., Proc. Int. Workshop Towards a Major Atmospheric Cherenkov Detector – II, Calgary (R.C. Lamb, Iowa State Univ., 1993) p. 235.
[11] T. Kifune et al., Proc. Int. Workshop Towards a Major Atmospheric Cherenkov Detector – II, Calgary (R.C. Lamb, Iowa State Univ., 1993) p. 39.
[12] F. Aharonian et al., Proc. XXII Int. Cosmic Ray Conf. 2, Dublin (1991) p. 615.
[13] M. Theshima, Proc. Int. Workshop on Techniques for the Study of Extremely High Energy Cosmic Rays, Tokyo (University of Tokyo, 1993) p.356.
[14] The EAS-TOP Coll. (M. Aglietta et al.), Proc. Int. Workshop Towards a Major Atmospheric Cherenkov Detector – I, Palaiseau, 1992, ed. P. Fleury and G. Vacanti (Editions Frontières, Gif-sur-Yvette, 1993) p. 221.
[15] R. DeSalvo et al., Nucl. Instr. Meth. A 315 (1992) 375.
[16] P. Fleury, Proc. Int. Workshop Towards a Major Atmospheric Cherenkov Detector – II, Calgary (R.C. Lamb, Iowa State Un., 1993) p. 188.
[17] The EAS-TOP Coll. (M. Aglietta et al.), Nuovo Cimento A 105 (1992) 1807.
[18] F. Aharonian et al., Proc. XXIII Int. Cosmic Ray Conf. 4, Calgary (1993) p. 291.
[19] A. Borione et al., Nucl. Instr. Meth. A 346 (1994) 329.
[20] The EAS-TOP Coll. (M. Aglietta et al.), Nuovo Cimento C 9 (1986) 262.
[21] The EAS-TOP Coll. (M. Aglietta et al.), Nucl. Instr. Meth. A 336 (1993) 310.
[22] A.M. Hillas, Proc. XIX Int. Cosmic Ray Conf. 3, La Jolla (1985) p. 445.
[23] The EAS-TOP Coll. (M. Aglietta et al.), Nuovo Cimento C 16 (1993) 813.
[24] The EAS-TOP Coll. (M. Aglietta et al.), Proc. Int. Workshop Towards a Major Atmospheric Cherenkov Detector – II, Calgary (R.C. Lamb, Iowa State Un., 1993) p. 66.
[25] The EAS-TOP Coll. (M. Aglietta et al.), Proc. XXIII Int. Cosmic Ray Conf. 4, Calgary (1993) p. 700.
[26] The EAS-TOP Coll. (M. Aglietta et al.), Proc. XXIV Int. Cosmic Ray Conf. 1, Roma (1995) p. 430.
[27] The EAS-TOP Coll. (M. Aglietta et al.), Proc. XXIV Int. Cosmic Ray Conf. 1, Roma (1995) p. 434.
[28] The EAS-TOP Coll. (M. Aglietta et al.), Proc. XXIV Int. Cosmic Ray Conf. 2, Roma (1995) p. 342.
[29] Philips Components, Data Handbook Photomultipliers PC04 (1989).
[30] GEANT: Detector Description and Simulation Tool, version 3.21, CERN W5013 Application Software Group and Network Division (1994).
[31] M. Hillas, J. Phys. G 8 (1982) 1475.
[32] D.A. Hill et al., Fifth Inter-American Seminar on Cosmic Rays, La Paz, Bolivia (1962).
[33] G. Bosia et al., Nature 225 (1970) 532.
[34] G. Bosia et al., Il Nuovo Cimento B 9 (1982) 177.
[35] G. Bosia et al., Il Nuovo Cimento C 3 (1980) 215.